DEFORMATION AND FRACTURE MODES OF SANDWICH STRUCTURES SUBJECTED TO UNDERWATER IMPULSIVE LOADS

L. F. Mori, S. Lee, Z. Y. Xue, A. Vaziri, D. T. Queheillalt,
K. P. Dharmasena, H. N. G. Wadley, J. W. Hutchinson and H. D. Espinosa

Sandwich panel structures with thin front faces and low relative density cores offer significant impulse mitigation possibilities provided panel fracture is avoided. Here steel square honeycomb and pyramidal truss core sandwich panels with core relative densities of 4% were made from a ductile stainless steel and tested under impulsive loads simulating underwater blasts. Fluid-structure interaction experiments were performed to (i) demonstrate the benefits of sandwich structures with respect to solid plates of equal weight per unit area, (ii) identify failure modes of such structures, and (iii) assess the accuracy of finite element models for simulating the dynamic structural response. Both sandwich structures showed a 30% reduction in the maximum panel deflection compared with a monolithic plate of identical mass per unit area. The failure modes consisted of core crushing, core node imprinting/punch through/tearing and stretching of the front face sheet for the pyramidal truss core panels. Finite element analyses, based on an orthotropic homogenized constitutive model, predict the overall structural response and in particular the maximum panel displacement.

1. Introduction

Structures that combine high stiffness, strength, and mechanical energy absorption with low weight, are widely used in a variety of aerospace, automotive, and Naval applications. Metallic sandwich panels with various light weight core topologies have attracted significant interest for shock mitigation in general and the mitigation of underwater propagated shocks in particular.

As a first step toward understanding the mechanical behavior of these types of sandwich structures, Chiras et al. [2002] and Rathbun et al. [2004] conducted quasistatic experiments and numerical simulations of the compressive and shear response of truss core panels with a tetragonal lattice topology. These studies identified an asymmetric structural response between compression loaded trusses collapsing by buckling and those placed in tension failing by fracture (usually near nodes). Rathbun et al. [2004] measured the behavior of tetrahedral truss sandwich panels in shear and bending. Deshpande and Fleck [2001] measured the collapse responses of truss core sandwich beams in 3-point bending and obtained upper bound expressions for the collapse loads. Wallach and Gibson [2001b] analyzed the elastic moduli and the uniaxial and shear strengths of a three-dimensional truss geometry. Other studies have addressed the role of structural core defects [Wallach and Gibson 2001a]. These studies were then used to motivate optimal design [Wicks and Hutchinson 2001; Rathbun et al. 2005] and to develop continuum constitutive models [Xue and Hutchinson 2004b]. Their compressive behavior has been measured by many groups and summarized and compared with honeycombs in [Wadley 2006].

The dynamic behavior of cores used in sandwich structures has also been extensively investigated. Vaughn et al. [2005] and Vaughn and Hutchinson [2006] performed numerical simulations of truss cores and quantified the effect of microinertia on load carrying capacity. Lee et al. [2006] analyzed the dynamic compressive behavior of pyramidal truss cores and showed that the material strain rate hardening and microinertia effects make significant contributions to the total energy absorbed by a core. A transition in failure mode with deformation rate was experimentally identified and numerically analyzed. The role of deformation rate on the crushing response of square honeycomb cores has been addressed theoretically by Xue and Hutchinson [2005] and for both folded plate and pyramidal truss cores by Vaziri and Xue [2007].

Extensive investigations of the fluid structure interaction (FSI) associated with shock impingement on a plate in both air and water were also pursued. The eventual application of these concepts will require full scale computational simulations. However, much computational power is required to conduct a complete fully core-gridded finite element analysis. Homogenized constitutive models are therefore being developed and implemented in finite element frameworks. Xue and Hutchinson [2003; 2004a] modeled circular truss cores sandwich plates subjected to uniformly distributed impulses with finite elements. The study extended the classical work of Taylor [1963] relating the far-field momentum to the momentum imparted to plates. The simulation results were then compared to those of solid plates made of the same material and having the same weight per unit area. They concluded a well-designed sandwich plate can sustain significantly larger impulses for a given maximum deflection. Moreover the analysis showed that, if the blast is under water, the fluid-structure interaction reduces the momentum transmitted to the sandwich plate by as much as a factor of two. Indeed, the fluid-structure interaction is predicted to enhance the performance of sandwich plates relative to solid plates under intense shocks even in air, in which the effects are thought not to be as significant as for water borne shocks [Vaziri and Hutchinson 2007].

Xue et al. [2005] proposed a homogenized constitutive model that incorporates rate-dependence arising from material rate-dependence and microinertial effects. The model was used with finite elements to represent the behavior of square honeycomb sandwich plates [Xue et al. 2005], folded plate and pyramidal truss cores [Vaziri and Xue 2007], and hexagonal honeycomb cores [Mohr et al. 2006] subjected to quasistatic and dynamic loads. Rabczuk et al. [2004] developed a homogenization method for sandwich structures using a quasicontinuum approach that takes into account buckling of the core; this model shows good agreement with fully discretized models for shell interlaced cores. Qiu et al. [2004; 2005a] developed an analytical model for the deformation response of clamped circular sandwich plates subjected to shock loading in air and in water. This model was verified using finite elements in [Qiu et al. 2003] and then used to define a systematic design procedure [Fleck and Deshpande 2004a].

Liang et al. [2007] used an analytic model based on the relative time scales for core crushing and water cavitation to evaluate the mechanical performance of different core topologies. The work highlighted the importance of core crushing strength for exploiting the benefits of fluid-structure interaction. Xue and Hutchinson [2005] developed a continuum model for high-rate deformation of square honeycomb cores and demonstrated that this is an effective core for sandwich plates because it combines excellent crushing strength and energy absorption with good out-of-plane stiffness and strength and in-plane stretching resistance. They also [Xue and Hutchinson 2004a; Hutchinson and Xue 2005] extended the work by Fleck and Deshpande [Fleck and Deshpande 2004b; Deshpande and Fleck 2005] and addressed the

problem of the minimum weight design of square honeycomb plates of given span that must sustain a uniformly distributed impulse. They argued that optimally designed sandwich plates could sustain water shocks that were two to three times larger than monolithic plates of the same mass and material. Further studies [Vaziri et al. 2007] investigated fracture modes of square honeycomb sandwich plates showing that the primary fracture modes are necking and subsequent tearing of the face sheets and webs, and shear delamination of the core webs from the faces. Vaziri et al. [2006] showed that there is no considerable advantage or disadvantage in filling the core interstices by low-density polymeric foams for structural purposes. Therefore, it is possible to exploit the multifunctional advantages offered by polymeric foam-filled cores, such as acoustic and thermal insulation, with only a minor weight penalty.

While all these analytical and computational models have been developed, experimental analysis of the structural behavior under blast loading is still limited. Radford et al. [2005] used Al foam projectiles fired from a gas gun at high velocities against stainless steel square honeycomb core sandwich panels. Although this technique produces pressure pulses representative of shock interactions caused by explosions [Radford et al. 2005; Qiu et al. 2005b; Rathbun et al. 2006], it cannot simulate the fluid-structure interaction (FSI), which is especially relevant for underwater explosions [Vaziri and Hutchinson 2007]. Hutchinson and Xue [2005], Liang et al. [2007] and Tilbrook et al. [2006] showed that much of the advantage of sandwich plates over solid plates subjected to underwater blast comes from the FSI and that optimal designs are highly dependant on the details of this interaction. Wave propagation in water and associated cavitation phenomena, which play an important role in FSI, make analytical and numerical modeling quite complex. Thus it is necessary to perform realistic FSI experiments to validate, calibrate, and develop models that take them into account. Wadley and his collaborators have investigated the structural response of lattice cores to shock loading in water and air [Dharmasena et al. 2007a; 2007b; Wadley et al. 2007a; 2007b]. The experiments confirm very significant reductions in the transmitted shock pressure and reduced panel deflections.

In this paper, a recently developed water shock tube technique similar to the one developed by Deshpande et al. [2006] is used to measure the dynamic structural response under a realistic, although scaled, fluid-structure interaction with a water borne shock [Espinosa et al. 2006]. Using this experimental setup, the dynamic performance of sandwich panels with honeycomb and pyramidal core topologies is compared with that of solid plates made of the same material under the same boundary conditions. Liang et al. [2007] introduced several performance metrics: the back-face deflection, the tearing susceptibility of the faces, and the loads transmitted to the supports. In this article, the performance of the different structures is compared in terms of the dynamic back-face deflection and the panel fracture modes. After describing the experimental technique and the design of the specimens, the experimental results for each kind of structure are presented; failure mechanisms in the sandwich panels are identified by exploring not only the maximum deflection but also the deformation history and the presence of fracture on the face sheets after the test. The experimental investigation is complemented by numerical simulations using a detailed computation model of the experimental setup. The model includes separate components representing the water column, tube, piston and sandwich plates, as will be described later. The core materials were modelled using a constitutive model, developed by Xue et al. [2005], for plastically orthotropic materials which allows for modelling nonuniform hardening and softening behavior in stressing in different directions. The validity of this constitutive model for simulating and predicting the structural response of sandwich plates underwater blast loading has been investigated by comparing the

experimental measurements and simulation predictions. The developed model was used to gain insight into the mechanism of deformation and the mechanics of sandwich plates subjected to underwater shock loading.

2. Methods

2.1. *Experimental approach.* A novel experimental methodology incorporating fluid-structure interaction (FSI) effects was recently developed [Lee 2005; Espinosa et al. 2006]. The set-up is a highly instrumented scaled model designed to characterize the underwater blast impulsive loading of structures and to identify their failure by means of real time measurements of deflection profiles, deformation histories, and fracture. In the FSI setup, a water chamber made of a steel tube is incorporated into a gas gun apparatus (Figure 1). A scaled structure is fixed at one end of the steel tube and a water piston seals the other end. A flyer plate impacts the water piston and produces an exponentially-decaying pressure history in lieu of blast loading caused by explosive detonation. The pressure induced by the flyer plate propagates and imposes an impulse to the structure (panel specimen), whose response elicits water cavitation. The performance of the set-up was assessed by conducting calibration experiments and by subjecting solid stainless steel panels to impulsive water loading. Pressure sensors were employed to record pressure histories. The experimental measurements confirmed that the FSI setup can generate an exponentially decaying pressure history. Shadow moiré and high speed photography were also used to record in real time the full field out-of-plane deformation profile of the solid panel [Lee 2005; Espinosa et al. 2006].

In this investigation the same setup has been employed. Stainless steel panel structures with square honeycomb and pyramidal truss cores were subjected to water borne shocks and assessed against monolithic plates using a maximum panel deflection metric. The mass per unit area of the sandwich structures is determined by the face sheet thickness and the core density. The tested sandwich panels had a relative density of 4% (see Table 1).
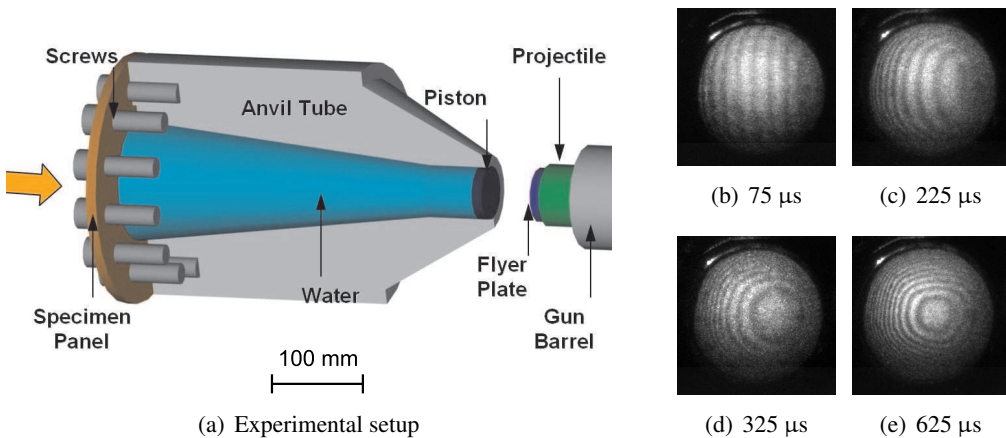

(a) Experimental setup

(b) 75 μs   (c) 225 μs

(d) 325 μs   (e) 625 μs

Figure 1. (a) Configuration of fluid-structure interaction (FSI) experimental setup. (b)–(e) Sequence of high-speed images obtained by shadow moiré.

Structure type	Core relative density	Mass per unit area, kg/m^2	Thickness, mm
Monolithic plate	100%	14.55	1.85
Square honeycomb sandwich	4.0%	14.00	13.97
Pyramidal truss sandwich	4.5%	13.78	12.75

Table 1. Properties of the edge clamped test specimens.

For each experiment, three loading parameters are of interest: the water pressure just ahead of the specimen panel, p_0, the characteristic decay time, t_0, and the far-field applied impulse, I_0. The incident transient load can be idealized as an exponentially decaying pressure given by:

$$p = p_0 \cdot e^{-t/t_0},$$

where p_0 is the peak water pressure measured in water just in front of the specimen panel and t_0 is a characteristic decay time [Smith and Hetherington 1994]. In the FSI setup, the peak pressure is governed by the projectile impact velocity, the acoustic impedance of the piston and the fluid, and by the experimental geometry (see Figure 1):

$$p_0 = V_0 \cdot \left(\frac{D_i}{D}\right)^2 \cdot \frac{s \cdot f}{s + f}, \tag{1}$$

where V_0 is the impact velocity, f and s are the acoustic impedances of the fluid and of the solid respectively, and D and D_i are the diameters of the water tube at the specimen and impact locations, respectively. Equation (1) has been derived using wave propagation theory with the assumption of linearity for the water equation of state [Espinosa et al. 2006]. Likewise, the time constant t_0 is obtained from evolving the nondimensional pressure profile in time:

$$\frac{p}{p_0} = e^{-t_n/t_0} = \left[\frac{s - f}{s + f}\right]^n, \qquad n = 0, 1, 2, \ldots.$$

In this equation, n is the number of wave reverberations in the flyer plate and t_n is the corresponding elapsed time. The far-field impulse I_0 per unit area is given by

$$I_0 = \sum_{n=0}^{\infty} p_0 \left[\frac{s - f}{s + f}\right]^n \Delta t \approx p_0 \cdot t_0,$$

where Δt is the time required for the elastic longitudinal wave to twice traverse the flyer plate [Espinosa et al. 2006].

To compare structures with different core geometries and materials, it is useful to employ the nondimensional impulse defined by Xue and Hutchinson [2004a] as

$$\hat{I} = \frac{I_0}{\overline{M} \cdot \sqrt{\sigma_y/\rho}},$$

where I_0 is the impulse per unit area previously defined, $\overline{M}$ the panel mass per unit area, σ_y the uniaxial tensile yield stress, and ρ the density of the specimen material.

Quantity	Symbol	Unit	Value
Young's modulus	E	GPa	200
Poisson's ratio	ν	–	0.3
Density	ρ_0	kg/m^3	7900
Melting temperature	T_{melt}	K	1673
Room temperature	T_{room}	K	293
Specific heat capacity	c	J/(kg·K)	440
Coefficient of thermal expansion	α	μm/(m·K)	17.3
Fitting parameter A	A	MPa	310
Fitting parameter B	B	MPa	1000
Fitting parameter n	n	–	0.65
Fitting parameter c	c	–	0.07
Fitting parameter $\dot{\varepsilon}_0$	$\dot{\varepsilon}_0$	s^{-1}	1.00
Fitting parameter m	m	–	1.00

Table 2. Material properties and Johnson–Cook parameters for AISI 304 stainless steel used in the numerical analyses.

3. Experimental results

3.1. *Honeycomb panels.*

3.1.1. *Specimen geometry.* The square honeycomb sandwich panels were fabricated from 304 stainless steel alloy, with an approximate composition of 67Fe-10Ni-20Cr-2Mn-1Si (wt%). The material properties for AISI 304 stainless steel are reported in Table 2. A slotted metal sheet assembly approach was used for fabrication [Wadley et al. 2003; Cote et al. 2004; Zok et al. 2004a; Wadley 2006]. Figure 2 schematically illustrates the fabrication sequence. First, a two dimensional profile was generated with a laser on a sheet metal strip incorporating the slots needed for the interlocking strip assembly and with allowances for bending the top and bottom flanges. The flanges were then bent at 90° to the core web. Finally, the core was assembled by slip fitting the laser cut and bent strips to form a square grid pattern. The core consisted of an assembly of 0.254 mm thick strips spaced 12.7 mm apart to form a 23 cell × 23 cell square grid (300 mm × 300 mm). A vacuum brazing method was used to bond 0.635 mm thick 304 stainless steel face sheets to the core to form the sandwich structure. The assemblies were vacuum brazed at an initial base pressure of $\sim$ 13 mPa. They were heated at 10 °C/min to 550 °C, held for 1 h (to volatilize the binder), then heated to the brazing temperature of 1050 °C, where they were held for 60 min at this temperature before furnace cooling at $\sim$ 25 °C/min to ambient. A braze alloy with a nominal composition of Ni-22.0Cr-6.0Si, wt.% (Nicrobraz® 31) was applied by spraying one side of the face sheet with a mixture of the braze powder and a polymer binder (Nicrobraz® 520 cement) which were both supplied by Wall Colmonoy (Madison Heights, WI).
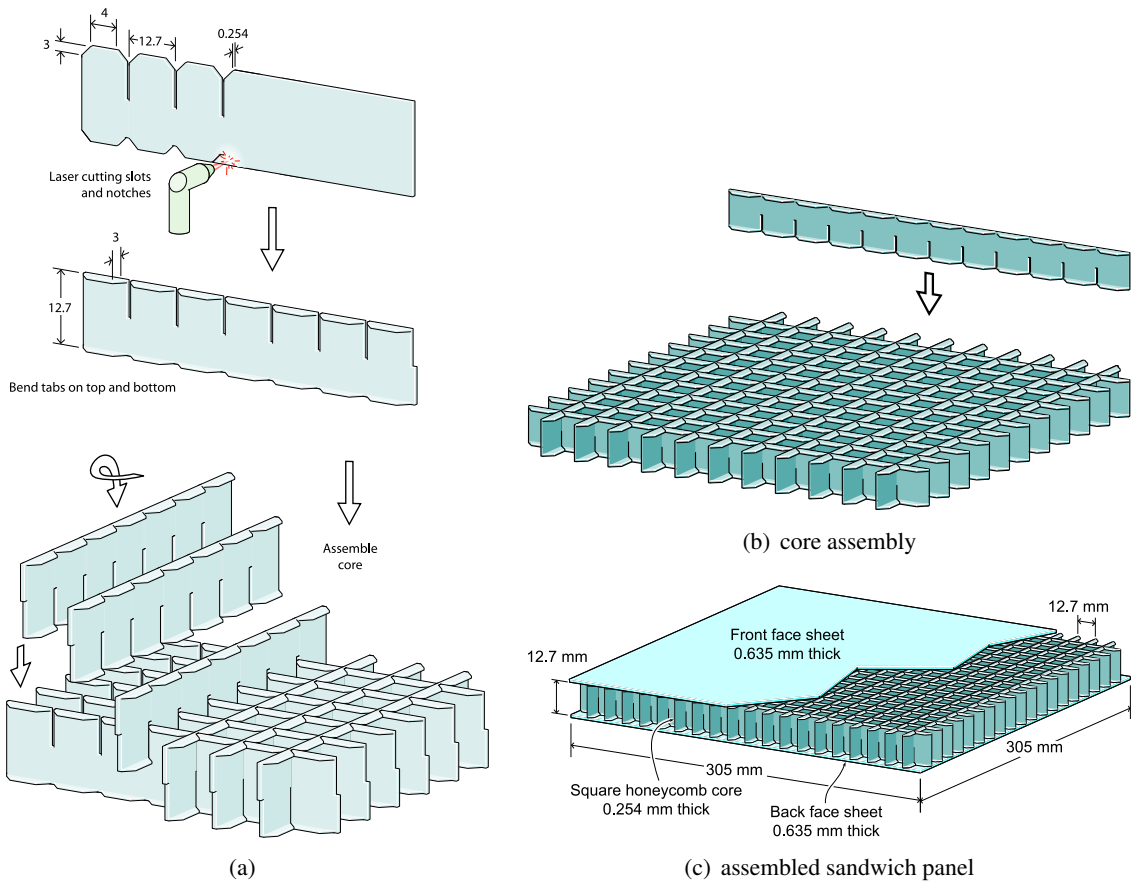
Figure 2. Fabrication of the square honeycomb sandwich panel by a transient liquid phase bonding process. All dimensions are in millimeters.

The panels were then machined to round specimens 305 mm in diameter (see Figure 3). The total thickness of the sandwich panels was 13.97 mm and the relative density of the core ρ_{cr} was 4%; the mass per unit area of the sandwich panels was 14.0 kg/m². To clamp the panels in the periphery, 12 through holes were machined and ring spacers were inserted to prevent core crushing during the clamping process. The specimens were clamped using a steel ring and 12 high strength screws.

Three experiments were conducted on the panels with projectile impact velocities between 175 m/s and 314 m/s. The results are summarized in Table 3. Details for the case with impact velocity of 272 m/s are given next.

3.1.2. *Test results: case with impact velocity of* 272 m/s. The peak pressure p_0 was 70.6 MPa; the characteristic decay time t_0 was 25.8 μs; the corresponding applied impulse I_0 was 30.16 N · s and the nondimensional applied impulse $\hat{I}$ was 1.234. The maximum deflection measured by shadow moiré, $\delta_{\max}$, was 29.62 mm and, thus, the nondimensional maximum deflection $\delta_{\max}/L$ was 0.389. The final strain of the core in the middle of the sample was $\varepsilon_f = 26.8\%$.
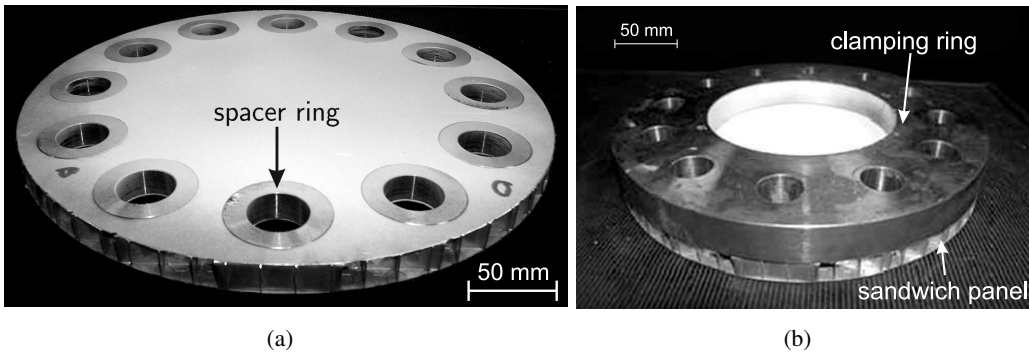
Figure 3. AISI 304 stainless steel panel with square honeycomb core. (a) Solid-ring spacers were employed to prevent core crushing while fastening the clamping ring. (b) A steel ring was employed to clamp the sandwich panel to the anvil tube with 12 screws. The test panel shown above is 305 mm in diameter and 13.97 mm thick.

Figure 4 shows the shadow moiré images between 25 μs and 625 μs after the wave front reached the specimen. The deflection along the diameter of the specimen obtained by processing the shadow moiré fringe patterns at different time instances is given in Figure 4i. Although no direct measurement of the back face velocity was performed, it is possible to compute an average velocity from the recorded history of the panel center position.

Figure 5 shows images of the honeycomb sandwich panel after the test. Square-grid imprints on both face sheets (see Figure 5a, b) are observed. The imprints on the face sheets are the result of the high crushing strength of the square honeycomb core. As discussed later, this phenomenon is characteristic of all the sandwich structures with a strong core. As observed in previous studies [Espinosa et al. 2006], the FSI configuration employing bolts to achieve a clamped boundary condition allows some in-plane

Structure type	Monolithic plate	Sandwich square honeycomb core			Sandwich pyramidal truss core
Impact velocity, V_0, m/s	315	175	272	314	307
Flyer plate thickness, t_f, mm	4.75	4.76	4.83	4.83	4.83
Water pressure, p_0, MPa	81.7	45.3	70.6	81.5	79.7
Characteristic decay time, t_0, μs	25.3	25.4	25.8	25.8	25.8
Final core strain, ε_f	—	1.7%	26.8%	7.1%	11.3%
Dimensionless applied impulse, $\hat{I}$	0.882	0.939*	1.234*	0.931	0.925
Dimensionless maximum deflection, δ_{max}/L	0.391	0.297	0.389	0.299	0.299
Normalized maximum deflection, $(\delta_{max}/L)_N$	0.391	0.279	0.278	0.283	0.285
Improvement	—	29%	29%	28%	27%
Damage on the face sheets	no damage	imprints			punctures/cracks

Table 3. Performances of blast-resistant structures with fixed boundary condition.

(a) 25 μs   (b) 75 μs   (c) 125 μs   (d) 175 μs

(e) 225 μs   (f) 325 μs   (g) 475 μs   (h) 625 μs
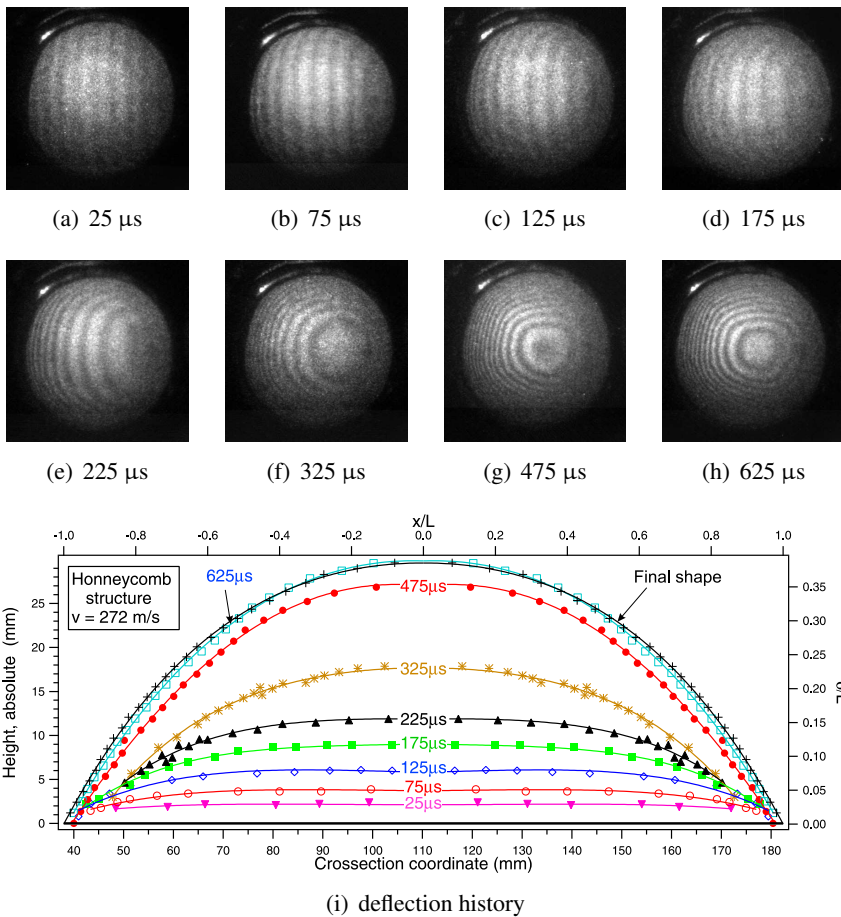
(i) deflection history

Figure 4. (a)–(h) High-speed camera images showing shadow moiré fringes for the AISI 304 stainless steel panel with square honeycomb core at different time intervals, and (i) deflection along the diameter of the specimen plate measured by shadow moiré. $t = 0$ μs corresponds to the arrival of the shock at the specimen location.

deformation of the sample at the boundary. Evidence of slippage and hole ovalization is reported in Figure 5d.

3.1.3. *Test results: comparison of the three experiments.* The three experiments that were conducted on the square honeycomb sandwich plates differ both in the speed of the projectile and on the geometry of the projectile. The external wall of the PMMA flyer holder was 8.5 mm-thick for the tests at 175 m/s and 272 m/s while it was 1.5 mm-thick for the test at 314 m/s. The additional impulse, for the cases of thicker holder tubes, was computed multiplying the compressive strength of PMMA, the cross-sectional area of the holder wall, and the time duration of the compressive stress wave propagation through the holder wall in the axial direction (for additional details see [Lee 2005]). With this correction, the tests at 175 m/s and at 314 m/s have almost the same nondimensional impulse (0.939 and 0.931) and in fact the final deflection is very similar (22.6 mm and 22.8 mm).
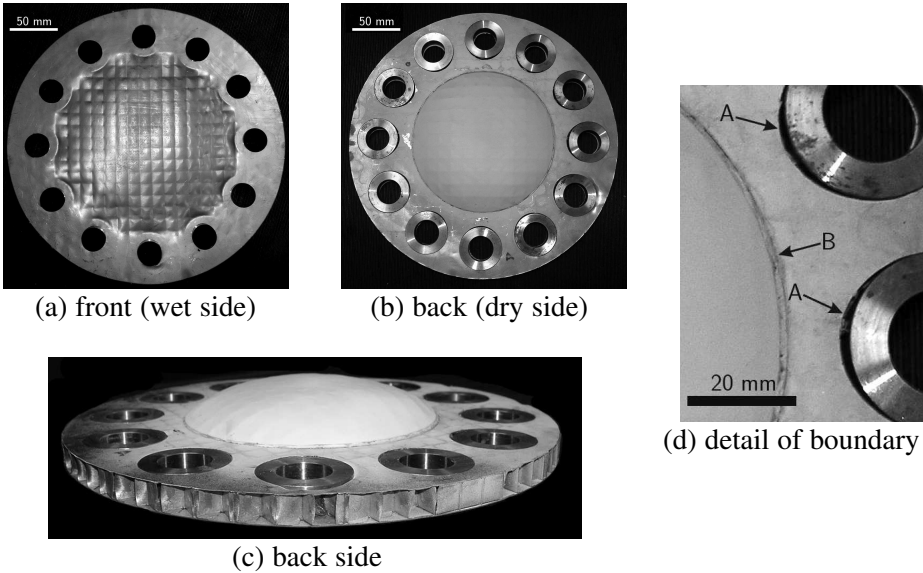
(a) front (wet side)   (b) back (dry side)

(d) detail of boundary

(c) back side

Figure 5. AISI 304 stainless steel honeycomb sandwich panel after the blast loading. (a), (b), and (c) show the front and the back of the plate while (d) shows details of hole ovalization (A) and slippage (B).

After the tests, the samples subjected to nondimensional impulses of $\hat{I} = 1.234$ and $\hat{I} = 0.939$ were cut in half by water-jet machining and are shown in Figure 6. On both cases significant core crushing close to the boundary is observed. However, the amount of core crushing in the center of the panel is very different. Only the largest impulse resulted in significant plastic buckling of the core webs in the center of the section panel (Figure 6b); the core buckled from the front (wet) side as shown in Figure 6e. The postmortem front and back face sheets profiles along the diameter of the panel subjected to a nondimensional impulse of $\hat{I} = 1.234$ are shown in Figure 7.

3.2. *Pyramidal lattice panels.*

3.2.1. *Specimen geometry.* Solid truss pyramidal lattice structures were fabricated via a folding operation that bends a diamond perforated sheet to create a single layer of trusses arranged with a pyramidal topology [Zok et al. 2004b; Queheillalt and Wadley 2005; McShane et al. 2006; Radford et al. 2006; Biagi and Bart-Smith 2007; Cote et al. 2007]. Briefly, the process consisted of punching a metal sheet to form a periodic diamond perforation pattern, folding node row by node row using a paired punch and die tool set, and then brazing this core to solid face sheets to form the sandwich structure. Figure 8 schematically illustrates this process. A solid truss structure with a core relative density of 4.5% was made from 304 stainless steel by the process described above. The sheet thickness $t = 1.52$ mm, truss width $w = 1.52$ mm, and the truss length $l = 17$ mm. The inclination angle $\omega = 45°$ and the face sheet thickness was 0.635 mm, resulting in a pyramidal lattice with square cross section trusses and a desired relative density.

(a) $\hat{I} = 0.939$, whole section

(b) $\hat{I} = 1.234$, whole section

(c) $\hat{I} = 0.939$, detail from the center

(d) $\hat{I} = 0.939$, detail from the boundary

(e) $\hat{I} = 1.234$, detail from the center

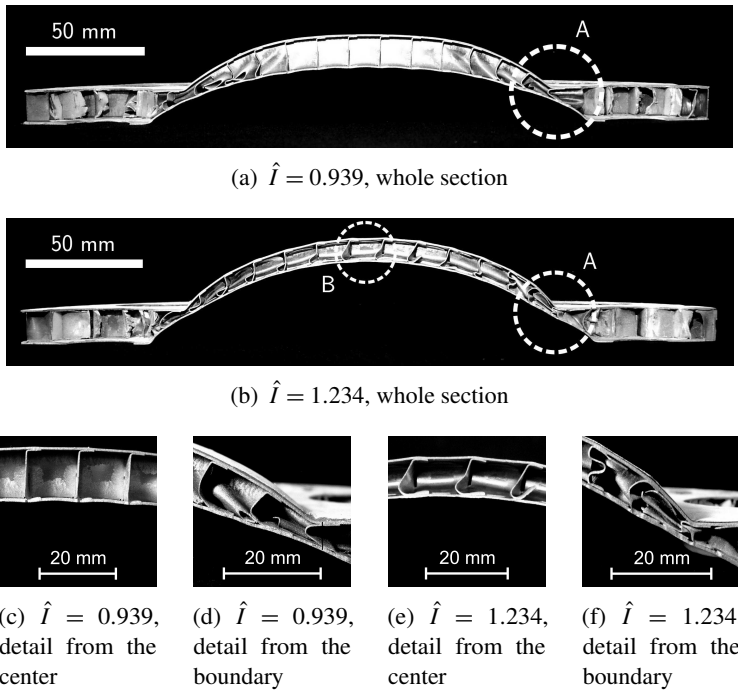(f) $\hat{I} = 1.234$, detail from the boundary

Figure 6. Cross-section of AISI 304 stainless steel honeycomb sandwich panels after blast loading. For the case of $\hat{I} = 0.939$, (a) core crushing occurs at the periphery, while for the case of $\hat{I} = 1.234$ (b) core crushing at both periphery (A) and center (B) occurs. (c)–(d) report core details for the lower impulse case and (e)–(f) for the higher impulse case.
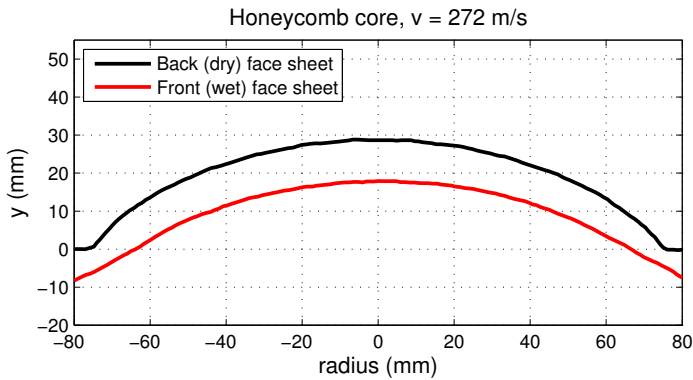
Figure 7. Postmortem profile of front and back face sheets along the diameter of the AISI 304 stainless steel panel with square honeycomb core subjected to a nondimensional impulse of $\hat{I} = 1.234$.
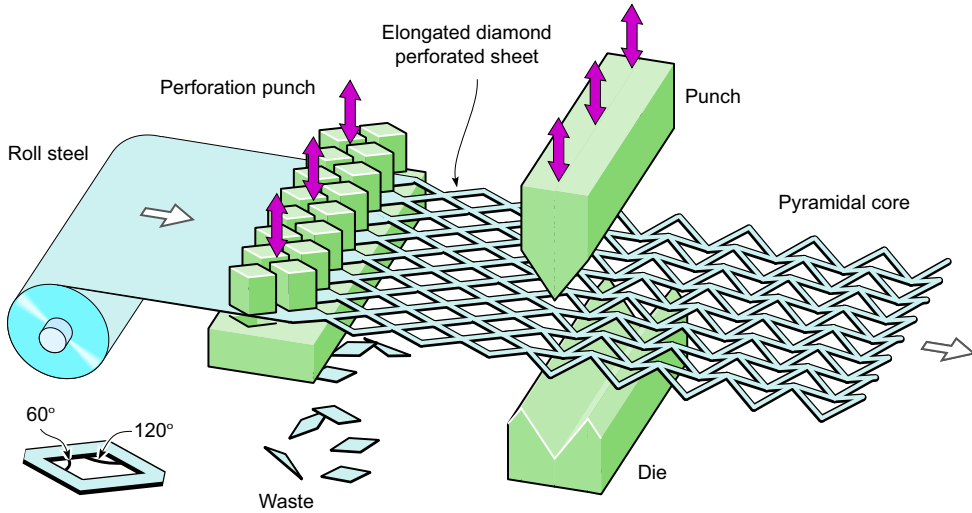
Figure 8. Fabrication of the pyramidal lattice core.

AISI 304 stainless steel panels with pyramidal truss cores were made by brazing the core to the face sheets. The brazing cycle for the truss core was the same as that previously described for the square honeycomb panels. The plates were then machined like the honeycomb panels to achieve the same boundary conditions. The overall thickness of the panels was 12.75 mm, the core relative density was 4.5% and the mass per area was 13.78 kg/m^2. The material properties for AISI 304 stainless steel are reported in Table 2.

3.2.2. *Test results.* The sandwich panel was tested at an impact velocity of 307 m/s using a flyer thickness of 4.83 mm and a PMMA flyer holder tube with wall thickness of 1.5 mm. This resulted in a peak pressure p_0 of 79.7 MPa and a characteristic decay time t_0 of 25.8 μs. The corresponding applied impulse I_0 was 37.47 N·s and the nondimensional applied impulse $\hat{I}$ was 0.925. The maximum deflection $\delta_{\max}$ was 22.79 mm, and thus the nondimensional maximum deflection $\delta_{\max}/L$ was 0.299. The final strain of the core in the middle of the sample was $\varepsilon_f = 11.3\%$.

Figures 9a–9h show fringe patterns, obtained by shadow moiré and high speed photography, at eight time instances between 93 μs and 793 μs after the wave front reached the specimen. The corresponding panel deflections along the diameter of the specimen are shown in Figure 9i.

Several distinct failure modes were observed in this experiment, as seen in Figures 10 and 11. Shear-off occurred at truss apexes on the front face sheet (wet side), (Figure 10a, c, and e). This failure mode is of main concern in sandwich panels with thin front face sheets and strong cores. On the other hand, the back face sheet partially sheared off at the supporting edge of the clamped boundary in Figure 10d and f. Ovalization of the holes and even fracture of the face sheet in the back was also observed in Figure 10b and d. The observed phenomena can be related to the influence of the boundary conditions and core properties.

After the experiment, the panel was sectioned and imaged as shown in Figure 11. Clearly, significant collapse of the pyramidal truss core is observed in the boundary region. The observed plastic buckling of the trusses is consistent with buckling modes at intermediate strain rates (see [Lee et al. 2006]). By
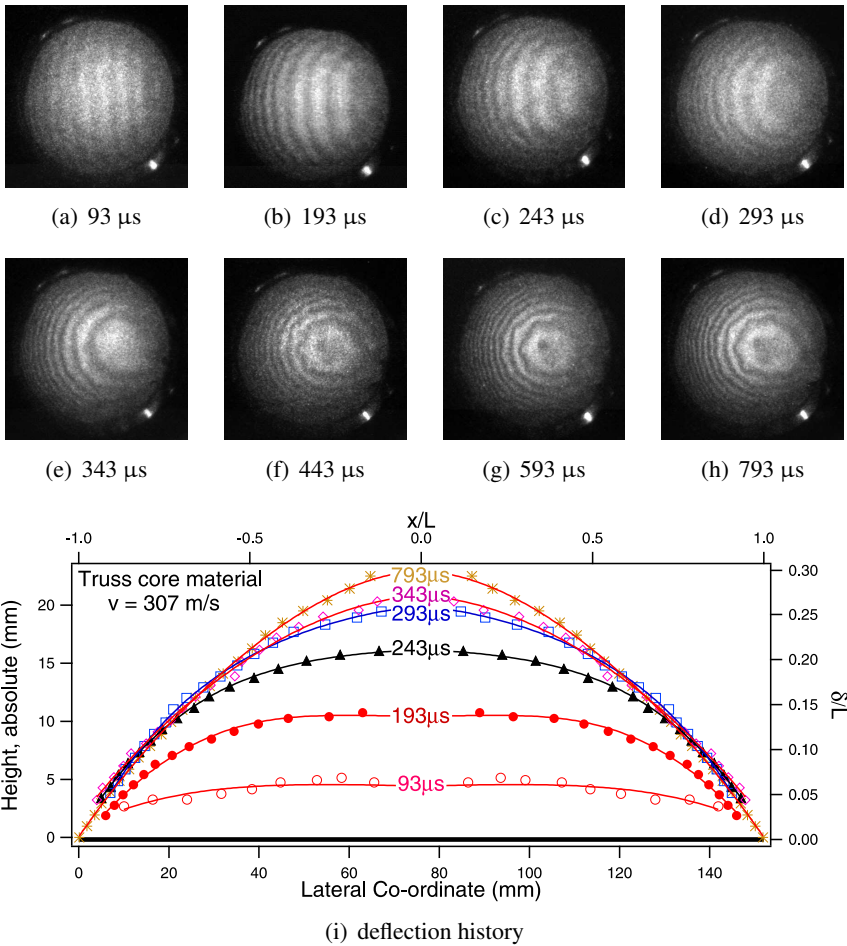
(a) 93 μs (b) 193 μs (c) 243 μs (d) 293 μs

(e) 343 μs (f) 443 μs (g) 593 μs (h) 793 μs

(i) deflection history

Figure 9. High-speed camera images of shadow moiré fringes for the AISI 304 stainless steel panel with pyramidal truss core at different time intervals (a)–(h), and deflection along the diameter of the specimen plate measured by shadow moiré (i). $t = 0$ μs corresponds to the arrival of the shock at the specimen location.

contrast, the core in the center of the specimen is almost undeformed, as shown in Figure 11a. The postmortem front and back face sheets profiles along the diameter of the panel are reported in Figure 12.

4. Comparison of Performances

As previously stated, comparison of performances is based on the nondimensional impulse $\hat{I}$ and the measured nondimensional maximum deflection $\delta_{\max}/L$. Since the experiments were performed at slightly different nondimensional impulses, all the results were referenced to one experiment. We chose the monolithic panel as our reference case such that any improvement by the sandwich topology automatically emerges. To scale the maximum deflection with impulse, we used the fact that nondimensional deflection
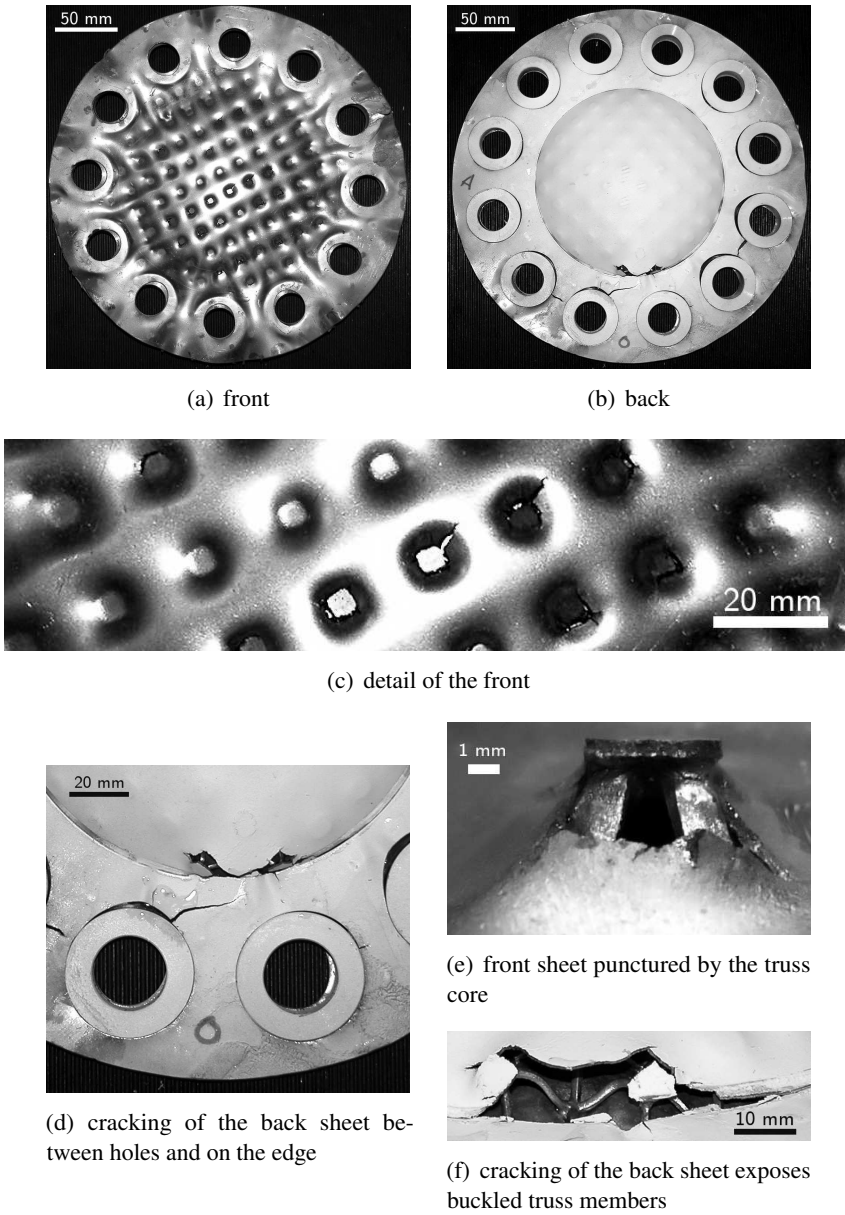
(a) front

(b) back

(c) detail of the front

(d) cracking of the back sheet be-
tween holes and on the edge

(e) front sheet punctured by the truss
core

(f) cracking of the back sheet exposes
buckled truss members

Figure 10. AISI 304 stainless steel sandwich panel with pyramidal truss core after blast loading. (a) and (b) and show the front and the back of the plate; (c) and (e) show details observed in (a). (d) and (f) show fracture features.

and impulse follow a linear relationship Xue and Hutchinson [2004a]. Then, the normalized maximum deflection is given by

$$(\delta_{\max}/L)_N = I_{nf} \cdot (\delta_{\max}/L)$$
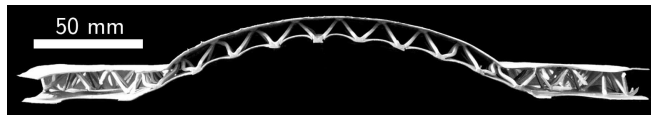
(a) cross-section
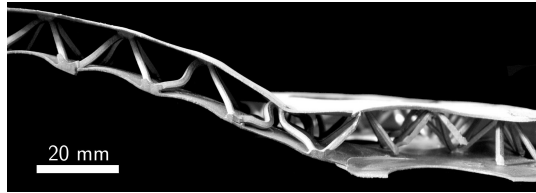
(b) detail of buckled truss members

Figure 11. Cross-section of AISI 304 stainless steel sandwich panel with pyramidal truss core after blast loading.

where I_{nf} is the impulse normalization factor defined as $I_{nf} \overset{\text{def}}{=} \frac{\hat{I}_{\text{monolithic}}}{\hat{I}}$.

The calculations and improvements are reported in Table 3. Both honeycomb and pyramidal truss cores exhibit an improvement of about 30%, with the pyramidal truss core presenting significant localized damage and lost of impermeability.

5. Numerical simulations

Finite element calculations using ABAQUS/Explicit 6.4–1 [2003] were carried out to mimic the response of the sandwich plates. As shown in Figure 13, an axisymmteric model of the experimental set up was developed.

The material of the anvil tube is wrought AISI 4340 steel, that of the specimen plate is AISI 304 stainless steel, and that of the piston and flyer plate is heat-treated AISI 4140 steel. For the anvil tube the strain hardening law $\sigma = K \cdot \varepsilon^n$ is used. For AISI 4340 steel an elastic-perfectly plastic model is used. The material properties and the strain hardening law parameters for the wrought AISI 4340 steel and for heat-treated AISI 4140 steel are given in Table 4. The anvil tube and the piston were modeled with 4-node axisymmetric elements with reduced integration. The von Mises criterion was adopted to model steel yielding.

The water was modeled as a hydrodynamic material and the following Mie–Grüneisen equation of state with a linear Hugoniot relation was used

$$ p = \frac{\rho_0 \cdot c_0^2 \cdot \eta}{(1 - s_1 \cdot \eta)^2} \cdot \left(1 - \frac{\Gamma_0 \cdot \eta}{2}\right) + \Gamma_0 \cdot \rho_0 \cdot E_m, \qquad u_s = c_0 + s_1 \cdot u_p. $$

A tensile pressure was made to correspond to water cavitation at room temperature. The material properties used in the simulation are listed in Table 5. The water was modeled with 3-node axisymmetric elements. Adaptive meshing was employed to prevent excessive element distortion in the water and a contact algorithm was incorporated to avoid penetration of steel surfaces. The amplitudes and overall
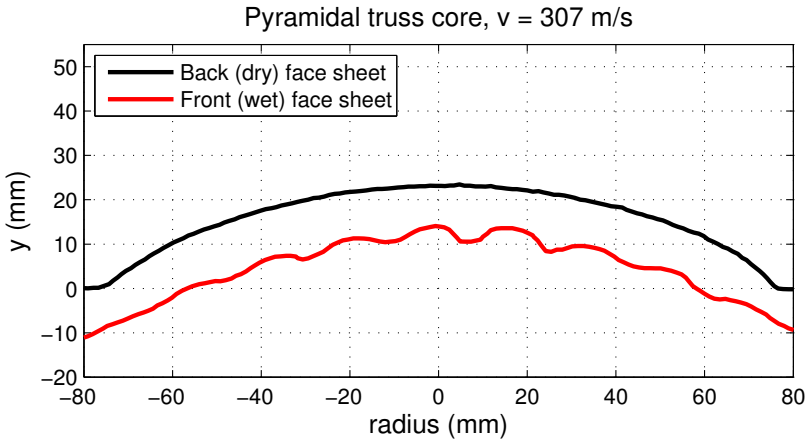
Figure 12. Postmortem profile of front and back face sheets along the diameter of the AISI 304 stainless steel panel with pyramidal truss core subjected to a nondimensional impulse of $\hat{I} = 0.925$.

Quantity	Symbol	Unit	AISI 4340 steel	AISI 4140 steel
Young's modulus	E	GPa	205	205
Poisson's ratio	ν	–	0.29	0.29
Density	ρ_0	kg/m^3	7850	7850
Yield stress	σ_0	MPa	470	1000
Hardening coefficient	K	MPa	470	1615
Hardening exponent	n	–	0	0.09

Table 4. Material properties and strain hardening coefficients for wrought AISI 4340 steel and for heat-treated AISI 4140 steel used in the numerical analyses.
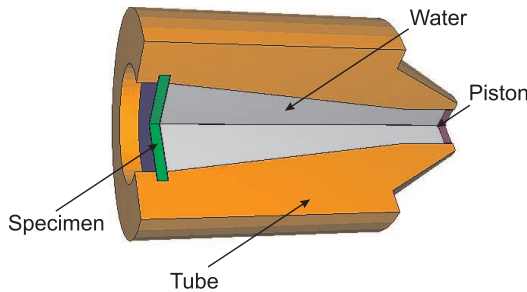

Figure 13. Schematic diagram of finite element model.

Quantity	Symbol	Unit	Water
Density	ρ_0	kg/m^3	958
Sound speed	c_0	m/s	1490
EOS coefficient	s_1	–	1.92
Grüneisen coefficient	Γ_0	–	0.1

Table 5. Material properties and parameters for the Mie–Grüneisen equation of state used for the water in the numerical analyses.

trends of pressure histories predicted by the model are in agreement with those measured in experiments [Espinosa et al. 2006].

The sandwich panels are made of stainless steel 304. The face sheets of the sandwich panel were meshed with 4-node axisymmetric elements with reduced integration. The Johnson–Cook plasticity model was adopted to model their elastic-plastic behavior. According to this model, the flow stress σ_y is given by

$$\sigma_y = \left[A + B \cdot \left(\varepsilon_p^{eq} \right)^n \right] \cdot \left(1 + c \cdot \ln \dot{\varepsilon}^* \right) \cdot \left[1 - \left(T^* \right)^m \right],$$

where

$$\dot{\varepsilon}^* \stackrel{\text{def}}{=} \frac{\dot{\varepsilon}_p^{eq}}{\dot{\varepsilon}_0}, \qquad T^* \stackrel{\text{def}}{=} \frac{T - T_{\text{room}}}{T_{\text{melt}} - T_{\text{room}}},$$

ε_p^{eq} and $\dot{\varepsilon}_p^{eq}$ are equivalent plastic strain and equivalent plastic strain rate, respectively; T is the material temperature, T_{room} is the room temperature, and T_{melt} is the melting temperature of the material; A, B,
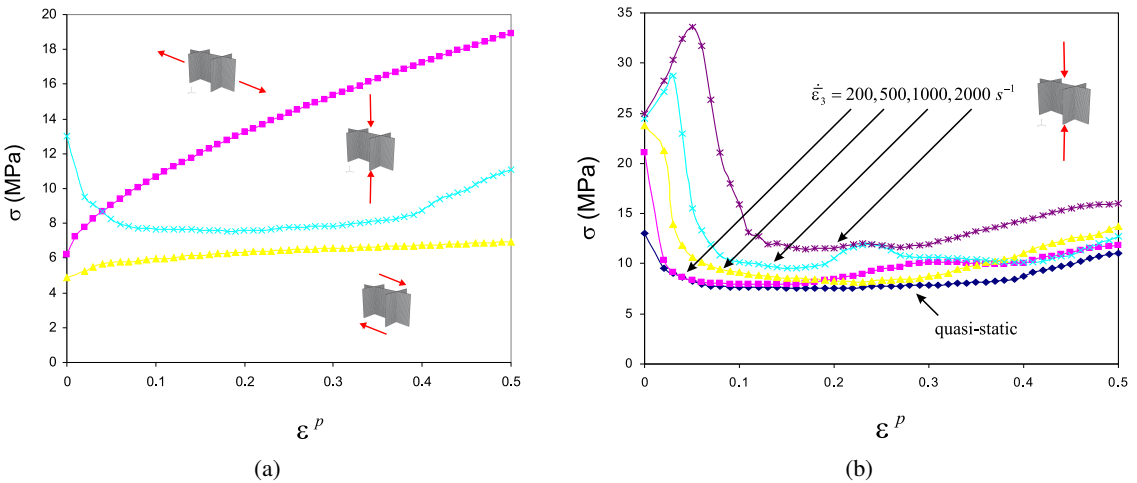

Figure 14. (a) True stress-plastic strain response of the square honeycomb core under three basic loading histories as computed using a three dimensional unit cell model. (b) Crushing response of the square honeycomb at various overall strain rates.
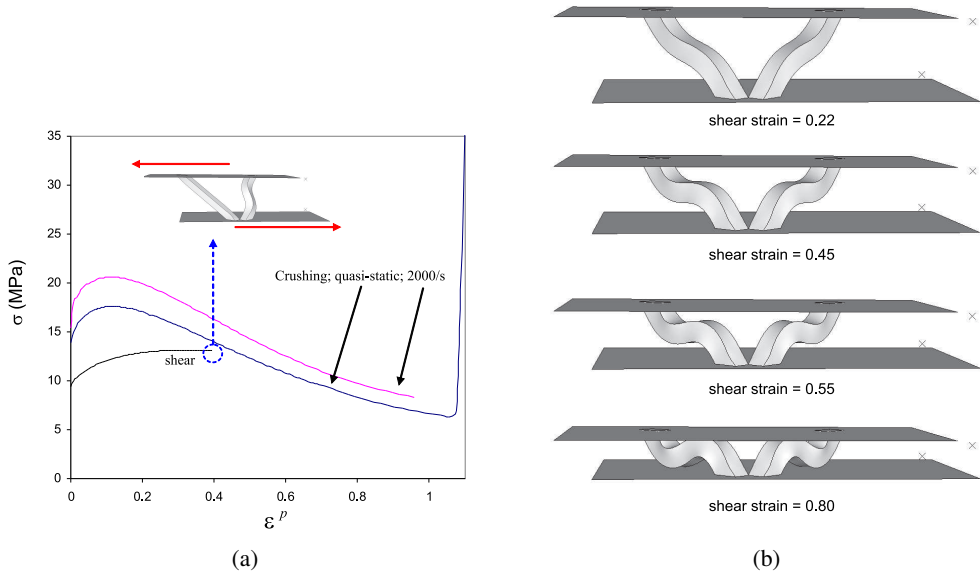
Figure 15. (a) True stress-plastic strain response of the square truss core under crushing and out of plane shearing as computed using the three dimensional unit cell model. The response of the truss core under a crushing rate of 2000/s is also depicted. Inset: deformed configuration of the truss core under out-of-plane shear at strain = 0.4. (b) Deformed configurations of the truss core under crushing at various level of crushing (true) strain.

n, c, $\dot{\varepsilon}_0$, and m are Johnson–Cook parameters determined by fitting experimental stress-strain curves as a function of strain rate and temperature. The material properties and the identified Johnson–Cook parameters for the AISI 304 stainless steel are listed in Table 2. The computational model of the core consists of a homogenized material using the orthotropic constitutive model developed by Xue et al. [2005]. Four-node axisymmetric elements with reduced integration were used for the core. The inputs to this constitutive model are rate-dependent stress-strain responses of the metal core under six fundamental loading histories. These inputs were calculated using full three-dimensional unit cell models of the two tested cores: square honeycomb and pyramidal truss. The unit cell calculations do not take into account any imperfection. The boundary conditions applied to the unit cell on the edges of the core webs are consistent with symmetry and periodicity. The details of the calculations are similar to those reported in [Xue et al. 2005; Vaziri and Xue 2007; Vaziri and Hutchinson 2007; Mohr et al. 2006]. The dimensions employed in the unit cell calculations were obtained from measurements on the tested panels.

Figure 14a shows the response of the square honeycomb core under crushing, out-of-plane shear, and in-plane stretching when deformed in the quasistatic regime. When the core is deformed at high strain rates, both material rate dependence and inertia effects could significantly alter its response. This effect is significant specifically under crushing where a combination of inertial resistance and delay in buckling leads to a significant enhancement in the crushing resistance of the core [Xue and Hutchinson 2005]. The response of the square honeycomb core under crushing at different strain rates are quantified in Figure
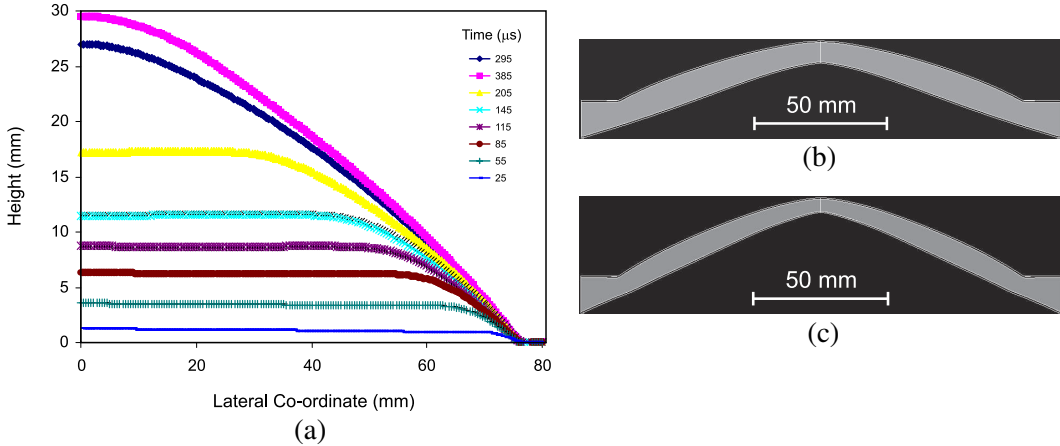
Figure 16. (a) Computed history of deformation of the dry-face sheet for the square honeycomb core sandwich panel (experimental results shown in Figure 4). (b) The final configuration of the square honeycomb core sandwich panel for the loading case $\hat{I} = 0.939$; experimental results are shown in Figure 6a. (c) The final configuration of the core sandwich panel for the loading case $\hat{I} = 1.234$; experimental results are shown in Figure 6b.

14b. These curves were directly input into the homogenized model to represent core behavior. All the calculations presented here incorporate the effect of deformation rate on core crushing. Its effect does not appear significant (see Figure 14b), in agreement with our previous studies [Xue et al. 2005; Vaziri and Xue 2007]. Similar calculations were carried out to quantify the response of the pyramidal truss core under three basic loading histories. The results of these calculations are summarized in Figure 15. For further discussion on deformation of pyramidal truss cores, see [Vaziri and Xue 2007].

In the computational model of the set up, the sandwich plate was taken to be perfectly bonded to the tube with an effective radius of 74 mm at its outer edge. The effect of the boundary condition will be discussed later. Frictionless contact was assumed at all other interfaces. The initial impulse per unit area $\bar{I}$ applied to the piston was experimentally measured. In the computational model, the impulse is simplified as a uniformly distributed velocity $v = \bar{I}/\rho h$ suddenly applied through the entire piston, where ρ and h denote the density and height of the piston.

6. Numerical results and discussion

The computed deflection histories of the dry side of the sandwich panel along its radial direction are shown in Figures 16a and 18a for the sandwich plates with square honeycomb core and pyramidal truss core. The corresponding experimental measurements are shown in Figures 4i and 9i. The maximum deflection history obtained with the FEM model is reported in Figures 17a and 19a for the sandwich plates with square honeycomb core and pyramidal truss core. Figure 19a shows an excellent agreement between numerical and experimental results. Figure 20 reports the comparison between the experimental result and the numerical prediction for the final shape of both types of sandwich structures. The difference in height between the prediction and the experimental result is less than 7% for the pyramidal truss core
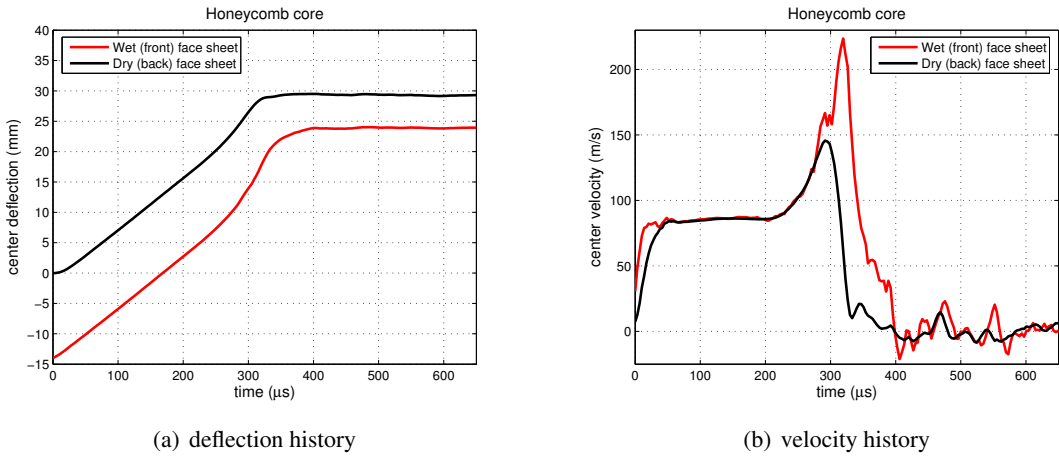
(a) deflection history

(b) velocity history

Figure 17. (a) Computed history of the maximum deflection of the dry-face and the wet face sheets for the square honeycomb core sandwich panel. (b) Computed history of the velocity of the center of the dry and wet face sheets after the Savitzky–Golay filter.
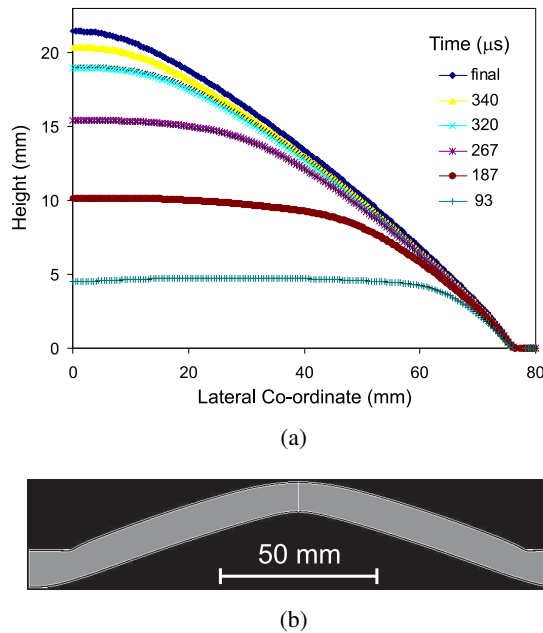

(a)

(b)

Figure 18. (a) Computed history of deformation of the dry-face sheet for the pyramidal truss core sandwich panel; experimental results are shown in Figure 9. (b) The final configuration of the pyramidal truss core sandwich panel; experimental results are shown in Figure 11.
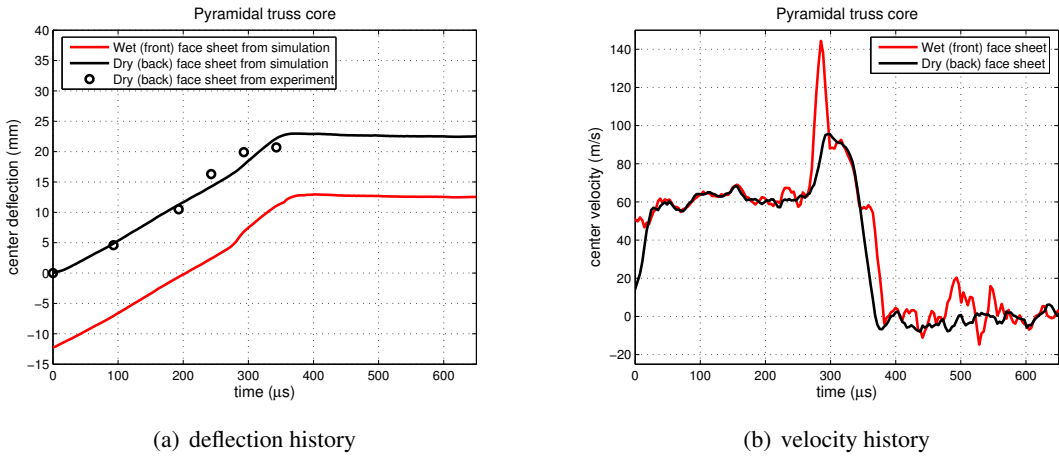
(a) deflection history

(b) velocity history

Figure 19. (a) Computed and experimental history of the maximum deflection of the dry-face and the wet face sheets for the pyramidal truss core sandwich panel. (b) Computed history of the velocity of the center of the dry and wet face sheets after the Savitzky–Golay filter.
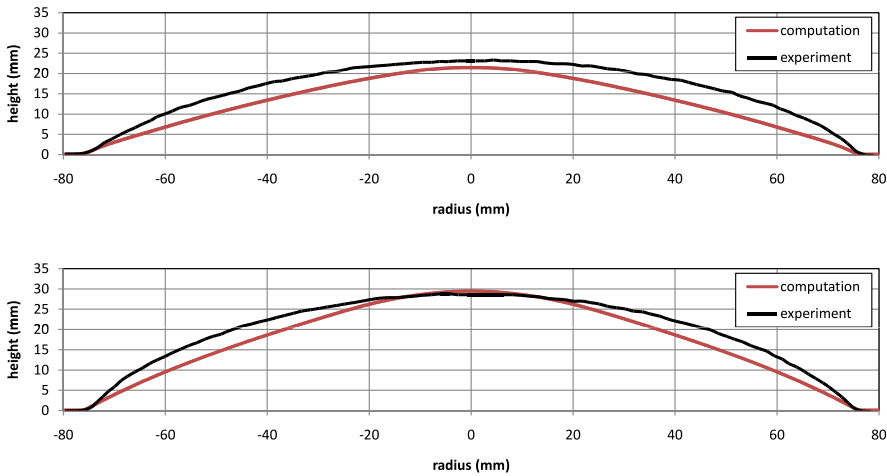

Figure 20. Comparison between the numerical prediction and the experimental result for the final shape of the pyramidal truss core sandwich (top) and the square honeycomb core sandwich (bottom).

and less than 3% for the square honeycomb. The velocity history of the center of the plate obtained with the FEM model is reported in Figure 17. Due to numerical errors of the FEM simulations, the velocity histories were noisy and so they were smoothed with a Savitzky–Golay filter on a frame of 10 points and with a polynomial of the third degree [Savitzky and Golay 1964]. The predicted deflection history profiles are in agreement with the corresponding experimental measurements. In particular, the

maximum deflection is captured very well by the computational model. A minor inconsistency between the numerical simulations and the experimental measurements is the time for the plate to attain a particular deformed shape. One possible reason is that the homogenization method fails to capture the full wave propagation process very accurately and slightly underpredicts the time interval required to achieve a given deformation. Figures 16b and 16c display the computed final deformed configuration of the sandwich panels with honeycomb cores for two impulses. Likewise, Figure 18b shows the computed final configuration for the case of pyramidal core. The results reveal a very good agreement between the experimental observations and numerical predictions, except that the crushing deformation of the sandwich panels around the edge is less in the numerical prediction. Noteworthy is that the 12 through holes machined on the panels, to achieve clamping, weaken the sandwich core locally and effectively act as imperfections. Since this feature was not accounted for in the numerical simulations, the local level of crushing observed experimentally was not reproduced by the simulations. Likewise, Figure 10 illustrates that tearing occurs on the face sheets of the sandwich panel with pyramidal truss cores in the clamped region. By contrast, the simulations did not account for fracture or rupture of the face sheets. Models capable of simulating fracture of metal sandwich plates are currently under development [Vaziri et al. 2007] and can be employed in the analysis of the experimental data in future studies. Due to the nature of the homogenization method, the numerical simulations also could not capture the local bending of the wet face due to shock loading at early stages of deformation. This local behavior is more pronounced for the panel with the truss core. Despite these limitations, the overall and maximum deflection are captured by the model in the spirit of its formulation.

7. Conclusions

A water shock tube has been used to investigate the fluid-structure interaction between water borne shock fronts and stainless steel sandwich panels with either honeycomb or pyramidal lattice cores of identical relative density. Tests have been conducted at impulse levels sufficient to initiate some of the panel failure modes. The panel deflections and back face velocity have been measured and compared with results obtained for monolithic panels of the same mass per unit area. A finite element modeling method has been used to investigate the basic deformation mechanisms of the core constituents and to predict the overall panel response to impulsive loading. We find that:

(i) The back face deflections of sandwich panels with specific mass of $14 \, \text{kg/m}^2$ subjected to impulse loading in the $1 - 2 \, \text{kPa} \cdot \text{s}$ range are approximately 30% less than those observed in solid panels of identical mass per unit area.

(ii) The difference in response partly resulted from reduced impulse acquired by the sandwich panels due to beneficial fluid-structure interactions. The simulations indicate that only a fraction of the far field impulse is transmitted to the structure.

(iii) The sandwich panels were also able to exhibit some core crushing (between 1.7 and 26.8% depending on core type and applied impulse) which also contributed to a reduction in FSI and energy dissipation.

(iv) The two core structures investigated underwent similar back (dry) face deflections. However, their front (wet) side deformation patterns were influenced by spacial distribution of nodal contacts with

the underlying core. The larger contact area for the honeycomb core resulted in slightly less face sheet stretching and tearing during the dynamic dishing of the panels.

(v) The resistance to face sheet tearing during impulse loading is clearly sensitive to the detailed design of the core-face sheet nodal contacts. Further work should explore approached for reducing the fracture susceptibility of the various candidate topologies.

Acknowledgments

References

[ABAQUS/Explicit 6.4–1 2003] ABAQUS/Explicit 6.4–1, *User's Manual*, ABAQUS Inc., 2003.

[Biagi and Bart-Smith 2007] R. Biagi and H. Bart-Smith, "Imperfection sensitivity of pyramidal core sandwich structures", *International Journal of Solids and Structures* **44**:14-15 (2007), 4690–4706.

[Chiras et al. 2002] S. Chiras, D. R. Mumm, A. G. Evans, N. Wicks, J. W. Hutchinson, K. Dharmasena, H. N. G. Wadley, and S. Fichter, "The structural performance of near-optimized truss core panels", *International Journal of Solids and Structures* **39** (2002), 4093–4115.

[Cote et al. 2004] F. Cote, V. S. Deshpande, N. A. Fleck, and A. G. Evans, "The out-of-plane compressive behavior of metallic honeycombs", *Materials Science and Engineering A* **380** (2004), 272–280.

[Cote et al. 2007] F. Cote, R. Biagi, H. Bart-Smith, and V. S. Deshpande, "Structural response of pyramidal core sandwich columns", *International Journal of Solids and Structures* **44**:10 (2007), 3533–3556.

[Deshpande and Fleck 2001] V. S. Deshpande and N. A. Fleck, "Collapse of truss core sandwich beams in 3-point bending", *International Journal Of Solids And Structures* **38**:36–37 (2001), 6275–6305.

[Deshpande and Fleck 2005] V. S. Deshpande and N. A. Fleck, "One-dimensional response of sandwich plates to underwater shock loading", *Journal Of The Mechanics And Physics Of Solids* **53**:11 (November 2005), 2347–2383.

[Deshpande et al. 2006] V. S. Deshpande, A. Heaver, and N. A. Fleck, "An underwater shock simulator", *Proceedings of the Royal Society A: Mathematical, Physical and Engineering Sciences* **462**:2067 (2006), 1021–1041.

[Dharmasena et al. 2007a] K. P. Dharmasena, D. T. Queheillalt, H. N. G. Wadley, Y. Chen, P. Dudt, D. Knight, Z. Wei, and A. G. Evans, "Dynamic response of a multilayer prismatic structure to impulsive loads incident from water", *International Journal of Impact Engineering* (2007). Accepted.

[Dharmasena et al. 2007b] K. P. Dharmasena, H. N. G. Wadley, Z. Y. Xue, and J. W. Hutchinson, "Mechanical response of metallic honeycomb sandwich panel structures to high intensity dynamic loading", *International Journal of Impact Engineering* (2007). In press.

[Espinosa et al. 2006] H. D. Espinosa, S. Lee, and N. Moldovan, "A Novel Fluid Structure Interaction Experiment to Investigate Deformation of Structural Elements Subjected to Impulsive Loading", *Experimental Mechanics* **46**:6 (2006), 805–824.

[Fleck and Deshpande 2004a] N. A. Fleck and V. S. Deshpande, "The Resistance of Clamped Sandwich Beams to Shock Loading", *Journal of Applied Mechanics* **71**:3 (2004), 386–401.

[Fleck and Deshpande 2004b] N. A. Fleck and V. S. Deshpande, "The resistance of clamped sandwich beams to shock loading", *Journal Of Applied Mechanics-Transactions Of The ASME* **71**:3 (May 2004), 386–401.

[Hutchinson and Xue 2005] J. W. Hutchinson and Z. Y. Xue, "Metal sandwich plates optimized for pressure impulses", *International Journal Of Mechanical Sciences* **47**:4–5 (April-May 2005), 545–569.

[Lee 2005] S. Lee, *Dynamic Failure of Blast-Resistant Structures Subjected to Impulsive Loading*, Ph.D. thesis, Northwestern University, Evanston, IL, USA, December 2005.

[Lee et al. 2006] S. Lee, F. Barthelat, J. W. Hutchinson, and H. D. Espinosa, "Dynamic failure of metallic pyramidal truss core materials: Experiments and modeling", *International Journal of Plasticity* **22**:11 (2006), 2118–2145.

[Liang et al. 2007] Y. Liang, A. V. Spuskanyuk, S. E. Flores, D. R. Hayhurst, J. W. Hutchinson, R. M. McMeeking, and A. G. Evans, "The Response Of Metallic Sandwich Panels To Water Blast", *Journal of Applied Mechanics* **74**:1 (2007), 81–99.

[McShane et al. 2006] G. J. McShane, D. D. Radford, V. S. Deshpande, and N. A. Fleck, "The response of clamped sandwich plates with lattice cores subjected to shock loading", *European Journal of Mechanics — A/Solids* **25** (2006), 215–229.

[Mohr et al. 2006] D. Mohr, Z. Y. Xue, and A. Vaziri, "Quasi-static punch indentation of a honeycomb sandwich plate: Experiments and Constitutive Modeling", *Journal of Mechanics of Materials and Structures* **1**:3 (2006), 581–604.

[Qiu et al. 2003] X. Qiu, V. S. Deshpande, and N. A. Fleck, "Finite element analysis of the dynamic response of clamped sandwich beams subject to shock loading", *European Journal Of Mechanics A-Solids* **22**:6 (November-December 2003), 801–814.

[Qiu et al. 2004] X. Qiu, V. S. Deshpande, and N. A. Fleck, "Dynamic response of a clamped circular sandwich plate subject to shock loading", *Journal Of Applied Mechanics-Transactions Of The ASME* **71**:5 (September 2004), 637–645.

[Qiu et al. 2005a] X. Qiu, V. S. Deshpande, and N. A. Fleck, "Impulsive loading of clamped monolithic and sandwich beams over a central patch", *Journal Of The Mechanics And Physics Of Solids* **53**:5 (May 2005), 1015–1046.

[Qiu et al. 2005b] X. Qiu, V. S. Deshpande, and N. A. Fleck, "Impulsive loading of clamped monolithic and sandwich beams over a central patch", *Journal of the Mechanics and Physics of solids* **53** (2005), 1015–1046.

[Queheillalt and Wadley 2005] D. T. Queheillalt and H. N. G. Wadley, "Pyramidal lattice truss structures with hollow trusses", *Materials Science and Engineering A* **397** (2005), 132–137.

[Rabczuk et al. 2004] T. Rabczuk, J. Y. Kim, E. Samaniego, and T. Belytschko, "Homogenization of sandwich structures", *International Journal For Numerical Methods In Engineering* **61** (2004), 1009–1027.

[Radford et al. 2005] D. D. Radford, V. S. Deshpande, and N. A. Fleck, "The use of metal foam projectiles to simulate shock loading on a structure", *International Journal of Impact Engineering* **31** (2005), 1152–1171.

[Radford et al. 2006] D. D. Radford, N. A. Fleck, and V. S. Deshpande, "The response of clamped sandwich beams subjected to shock loading", *International Journal of Impact Engineering* **32** (2006), 968–987.

[Rathbun et al. 2004] H. J. Rathbun, Z. Wei, M. Y. He, F. W. Zok, A. G. Evans, D. J. Sypeck, and H. N. G. Wadley, "Measurement and Simulation of the Performance of a Lightweight Metallic Sandwich Structure With a Tetrahedral Truss Core", *Journal of Applied Mechanics* **71**:3 (2004), 368–374.

[Rathbun et al. 2005] H. J. Rathbun, F. W. Zok, and A. G. Evans, "Strength optimization of metallic sandwich panels subject to bending", *International Journal of Solids and Structures* **42**:26 (2005), 6643–6661.

[Rathbun et al. 2006] H. J. Rathbun, D. D. Rodford, Z. Y. Xue, M. Y. He, J. Yang, V. Deshpande, N. A. Fleck, J. W. Hutchinson, F. W. Zok, and A. G. Evans, "Performance of metallic honeycomb-core sandwich beams under shock loading", *International Journal of Solids and Structures* **43** (2006), 1746–1763.

[Savitzky and Golay 1964] A. Savitzky and M. J. E. Golay, "Smoothing and differentiation of data by simplified least squares procedures", *Analytical Chemistry* **36**:8 (1964), 1627–1639.

[Smith and Hetherington 1994] P. D. Smith and J. G. Hetherington, *Blast and ballistic loading of structures*, Butterworth-Heinemann, Oxford, November 1994.

[Taylor 1963] G. I. Taylor, *The scientific papers of G. I. Taylor*, vol. III, Chapter The pressure and impulse of submarine explosion waves on plates, pp. 287–303, Cambridge University Press, Cambridge, 1963.

[Tilbrook et al. 2006] M. T. Tilbrook, V. S. Deshpande, and N. A. Fleck, "The impulsive response of sandwich beams: analytical and numerical investigation of regimes of behaviour", *Journal of the Mechanics and Physics of Solids* **54**:11 (2006), 2242–2280.

[Vaughn and Hutchinson 2006] D. G. Vaughn and J. W. Hutchinson, "Bucklewaves", *European Journal of Mechanics A-Solids* **25**:1 (2006), 1–12.

[Vaughn et al. 2005] D. G. Vaughn, J. M. Canning, and J. W. Hutchinson, "Coupled plastic wave propagation and column buckling", *Journal of Applied Mechanics* **72**:1 (2005), 139–146.

[Vaziri and Hutchinson 2007] A. Vaziri and J. W. Hutchinson, "Metallic sandwich plates subject to intense air shocks", *International Journal of Solids and Structures* **44**:1 (2007), 2021–2035.

[Vaziri and Xue 2007] A. Vaziri and Z. Y. Xue, "Mechanical behavior and constitutive modeling of metal cores", *Journal of Mechanics of Materials and Structures* **2**:9 (2007), 1743–1760. In press.

[Vaziri et al. 2006] A. Vaziri, Z. Y. Xue, and J. W. Hutchinson, "Metal sandwich plates with polymeric foam-filled cores", *Journal of Mechanics of Materials and Structures* **1**:1 (2006), 95–128.

[Vaziri et al. 2007] A. Vaziri, Z. Y. Xue, and J. W. Hutchinson, "Performance and failure of metal sandwich plates subject to shock loading", *Journal of Mechanics of Materials and Structures* (2007). In press.

[Wadley 2006] H. N. G. Wadley, "Multifunctional periodic cellular metals", *Philosophical Transactions of the Royal Society A* **364** (2006), 31–68.

[Wadley et al. 2003] H. N. G. Wadley, N. A. Fleck, and A. G. Evans, "Fabrication and structural performance of periodic cellular metal sandwich structures", *Composite Science & Technology* **63** (2003), 2331–2343.

[Wadley et al. 2007a] H. N. G. Wadley, K. P. Dharmasena, Y. Chen, P. Dudt, D. Knight, R. Charette, and K. Kiddy, "Compressive response of multilayered pyramidal lattices during underwater shock loading", *International Journal of Impact Engineering* (2007). In press.

[Wadley et al. 2007b] H. N. G. Wadley, K. P. Dharmasena, D. T. Queheillalt, Y. Chen, P. Dudt, D. Knight, K. Kiddy, Z. Xue, and A. Vaziri, "Dynamic compression of square honeycomb structures during underwater impulsive loading", *Journal of Mechanics of Materials and Structures* (2007). In press.

[Wallach and Gibson 2001a] J. C. Wallach and L. J. Gibson, "Defect sensitivity of a 3D truss material", *Scripta Materialia* **45**:6 (2001), 639–644.

[Wallach and Gibson 2001b] J. C. Wallach and L. J. Gibson, "Mechanical behavior of a three-dimensional truss material", *International Journal of Solids and Structures* **38** (2001), 7181–7196(16).

[Wicks and Hutchinson 2001] N. Wicks and J. W. Hutchinson, "Optimal truss plates", *International Journal of Solids and Structures* **38**:30–31 (2001), 5165–5183.

[Xue and Hutchinson 2003] Z. Y. Xue and J. W. Hutchinson, "Preliminary assessment of sandwich plates subject to blast loads", *International Journal Of Mechanical Sciences* **45**:4 (April 2003), 687–705.

[Xue and Hutchinson 2004a] Z. Y. Xue and J. W. Hutchinson, "A comparative study of impulse-resistant metal sandwich plates", *International Journal of Impact Engineering* **30**:10 (November 2004), 1283–1305.

[Xue and Hutchinson 2004b] Z. Y. Xue and J. W. Hutchinson, "Constitutive model for quasi-static deformation of metallic sandwich cores", *International Journal For Numerical Methods In Engineering* **61** (2004), 2205–2238.

[Xue and Hutchinson 2005] Z. Y. Xue and J. W. Hutchinson, "Crush dynamics of square honeycomb sandwich cores", *International Journal for Numerical Methods in Engineering* **65** (2005), 2221–2245.

[Xue et al. 2005] Z. Y. Xue, A. Vaziri, and J. W. Hutchinson, "Non-uniform constitutive model for compressible orthotropic materials with application to sandwich plate cores", *Computer Modeling in Engineering & Sciences* **10**:1 (2005), 79–95.

[Zok et al. 2004a] F. W. Zok, H. Rathbun, M. He, E. Ferri, C. Mercer, R. M. McMeeking, and A. G. Evans, "Structural performance of metallic sandwich panels with square honeycomb cores", *Philosophical Magazine* **85** (2004), 3207–3234.

[Zok et al. 2004b] F. W. Zok, S. A. Waltner, Z. Wei, H. J. Rathbun, R. M. McMeeking, and A. G. Evans, "A protocol for characterizing the structural performance of metallic sandwich panels: application to pyramidal truss cores", *International Journal of Solids and Structures* **41** (2004), 6249–6271.

L. F. MORI: lapo.mori@gmail.com
Department of Mechanical Engineering, Northwestern University, Evanston, IL 60208, United States

S. LEE: sungsoo.f.lee@gmail.com
Department of Mechanical Engineering, Northwestern University, Evanston, IL 60208, United States

Z. Y. XUE: xue@deas.harvard.edu
School of Engineering and Applied Sciences, Harvard University, Cambridge, MA 02138, United States

A. VAZIRI: avaziri@deas.harvard.edu
School of Engineering and Applied Sciences, Harvard University, Cambridge, MA 02138, United States

D. T. QUEHEILLALT: dtq2j@virginia.edu
Department of Materials Science and Engineering, University of Virginia, 140 Chemistry Way, Charlottesville, VA 22904, United States

K. P. DHARMASENA: kumar@virginia.edu
Department of Materials Science and Engineering, University of Virginia, 140 Chemistry Way, Charlottesville, VA 22904, United States

H. N. G. WADLEY: haydn@virginia.edu
Department of Materials Science and Engineering, University of Virginia, 140 Chemistry Way, Charlottesville, VA 22904, United States

J. W. HUTCHINSON: jhutchin@fas.harvard.edu
School of Engineering and Applied Sciences, Harvard University, Cambridge, MA 02138, United States

H. D. ESPINOSA: espinosa@northwestern.edu
Department of Mechanical Engineering, Northwestern University, Evanston, IL 60208, United States